



A New Wide Tunability MEMS Based Variable Capacitor using Two Separate Electrostatic Vertical Comb Drive Actuators

M. Ghalandarzadeh, S. Afrang*

Electrical Engineering Department, Faculty of Engineering, Urmia University, Urmia, Iran

PAPER INFO

Paper history:

Received 06 September 2020

Received in revised form 23 September 2021

Accepted 01 October 2021

Keywords:

MEMS

Variable Capacitors

Tunability

Electrostatic

Vertical Comb Drives

Pull-in

ABSTRACT

This paper presents a new MEMS variable capacitor to achieve high stable region and extremely wide tunability. The idea is based on increasing the stable region in the gap between the plates of the capacitor. It is done by combining the functionality of two different vertical comb drive actuator sets to takeover a unity air gap variation. The design of the structure is carried out so that the performance of these two actuator sets is fully independent without any destructive or damaging effect on each other. The advantage of this scheme is that adding the second mechanism of actuation does not change the overall structure thickness compared with when the structure uses a single actuation mechanism. Therefore, the tunability increases sharply. Aluminum is the structural material used for the design. Comb actuators are widely used as MEMS motors due to their long range of linear motion, low power consumption and ease of fabrication. A full review of electrostatic actuator portion is done. The structure is calculated using MATLAB software. To verify, the calculated results were compared with simulated results using Intellisuite software. The natural frequency is 1.173 KHz. According to calculation and simulation results the achieved minimum tuning range is 2300%.

Doi: 10.5829/ije.2021.34.11b.16

1. INTRODUCTION

MEMS-based variable capacitors are used as key building blocks in many wireless communication applications, such as tunable filters, voltage-control oscillators, matching networks and phase shifters [1-4]. Commercially available solid-state varactors such as p-n junction diodes and Schottky diodes offer wide tuning range, small size and very fast tuning speed [5]. However, they suffer from low power handling, low Q-factor and non-linearity effect.

Compared to semiconductor varactors, MEMS variable capacitors have the potential for an extended tuning range, higher linearity and high quality factor [6-12], along with the reduction in weight, size, and cost of communication systems. According to working principle, the popular actuators for MEMS variable capacitors can be mainly classified into three categories, which include electrothermal, piezo-electric, and

electrostatic actuators. Thermally and piezoelectrically actuated devices provide great motion control. Very linear variable capacitors can be obtained this way, and a few have been reported [13-16]. However, some of the major concerns are the hysteresis in actuation motion, power consumption, and response time. On the other hand, electrostatic actuation remains an attractive method for actuation the tuning capacitors due to virtually nonexistent current loss, high energy density, low power consumption and high-quality factors and large force that can be generated on the microscale [17, 18].

Micromachined variable capacitors generally fall in two categories those that vary the area and those that vary gap [17, 19]. Often, gap-tuning capacitors are constructed from two surface-micromachined electrostatically actuated parallel plates, one being movable and controlled by an applied voltage and the other being fixed [20-23]. The main problem in the electrostatic type variable capacitor is the pull in instability. This

*Corresponding Author Institutional Email: s.afrang@urmia.ac.ir (S. Afrang)

phenomenon limits the range of tuning [24-29]. The movable plate can only be actuated one third of the initial gap distance; beyond this value, the two plates will snap together. This phenomena can be explained by the mechanical instability between electrostatic forces and restoring forces of the varactor structure, which causes the upper plate to snap down when it reaches one-third of the air gap [2, 13]. In this case, the maximum theoretical tuning ratio is only 1.5:1. Although, techniques that increase the tuning range have been reported, they often do not have tuning ratios large enough for many RF applications, and furthermore, have increased process complexity. Recently, several approaches have been reported to enhance the tuning range of variable capacitors. The approaches involve either parallel plate capacitors and actuators [30-34] or interdigitate capacitors with comb drive actuation mechanisms [10, 35]. The parallel-plate capacitor with electro-static actuation that is preferable due to its high self-resonance, high quality factor, low power consumption and the interdigitated capacitors that have a linear response, but exhibit a low selfresonance and low quality factor.

Comb drive structures can be widely used in electrostatically actuated MEMS devices. In this paper, we present a surface-micromachined variable capacitor that employs two sets of comb drive actuators to vertically displace parallel plate capacitors. The main aim of this article is to introduce a new structure to achieve variable capacitor with large tuning range using electrostatic actuators. In the comb drive electrostatic actuators, the pull in instability occurs later than conventional parallel plate electrostatic actuators [36]. A particular type of a comb drives are made vertically and are known as vertically comb drives. As mentioned, we lose nearly half of the air gap because of the phenomenon of pull-in.

We have proposed a new structure to overcome this problem, and achieve very large tuning range. Based on the proposed structure, we have introduced two steps of displacement. At the first step or phase I, half of the desired displacement is done by the first group of vertical comb drive actuators. this step will stop when it comes to pull in instability point. Then at the second step or phase II and for the first time, the other half of the desired displacement becomes realized by the second group of vertical comb drive actuators. In fact, using the second group of comb drives, the first pull-in point is eradicated and we were able to capture the entire air gap to obtain maximum tuning range. Therefore, the tuning range of the variable capacitor is sharply increased.

2. DEVICE STRUCTURE

The schematic diagram of the proposed structure is shown in Figures 1 (Top view) and 2 (Button view).

The structure consists of two sets of movable and fix comb drives (the outer side), four sets of movable and fix comb drives (the inner side), four fixed-guided end beams as springs (the outer side), four fixed-guided end beams as springs (the inner side), two stoppers, frame, four anchors and two parallel plates as the desired capacitor.

The anchors are 4 in number and in the corners of the structure. The upper part of the structure, including the frame, outer springs, inner springs, outer comb drives, inner comb drives and up capacitor plate are all held in a suspended state on these anchors at a certain distance from the bottom structure. The anchors are connected from the bottom to the substrate and from the top to the external springs.

The lower plate of the capacitor is fixed to the substrate and upper plate is suspended by inner fixed-guided end beams. The plates are precisely opposite each other and at a distance as a gap (g) from each other.

The movable plate together with fixed plate makes the proposed variable capacitor. The frame is the interface between the outer and the inner springs. Outer springs from the side of guided-end and the inner springs are attached to the fix frame.

As shown in Figure 3, the outer movable combs are connected to the bottom of the frame and they move

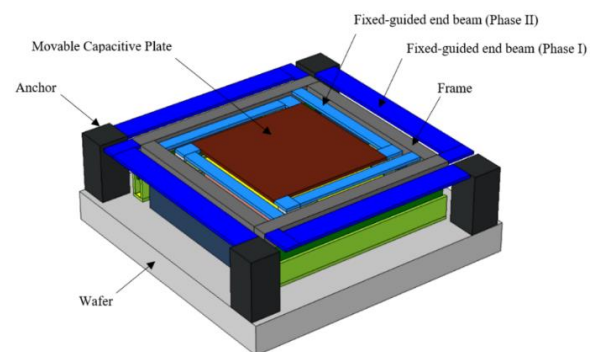


Figure 1. The schematic of the proposed variable capacitor (Top view)

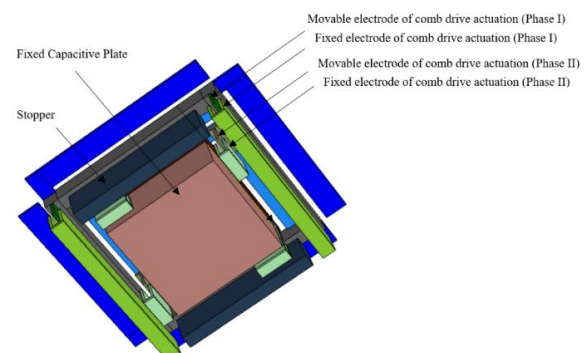


Figure 2. The schematic of the proposed variable capacitor (Button view)

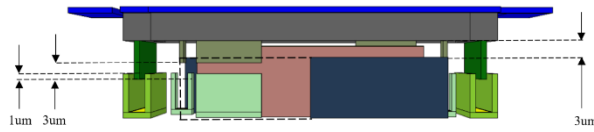


Figure 3. Location of inner and outer comb drive actuators

downward by the external springs, whereas, the inner movable combs are placed under the guided-end side of the inner springs and moved downward by the inner springs. The two stoppers are located at the bottom of the other sides of the frame.

The proposed variable capacitor has a wide range of capacitive variation. In order to realize this, two separate electrostatic actuation mechanisms are used.

In phase I, by applying voltage to the external comb actuators, the frame together with inner spring and upper capacitor plate is moved downward by the outer springs. After $\frac{g}{2}$ displacement, the frame stop by the stoppers. At this moment, the first displacement mechanism ends. If we assume that the air gap between the front end of external comb drives is g in the initial state, then at the end of phase I this distance has reached $\frac{g}{2}$.

In general, when the actuation voltage is applied to the comb drives, the electrostatic force generated in the comb drives moves the upper plate downward. This generated electrostatic force is more linear than the conventional electrostatic force, produced by the parallel-plate actuator. Moreover, this technique postpones the pull-in behavior compared to conventional parallel plate capacitors. Therefore, allows the movable plate to continue moving down linearly and consequently increase the tunability range of the variable capacitor. In the pull in point the equivalent stiffness of the structure becomes zero and leads the system to an unstable condition by undergoing to a saddle node bifurcation. In the proposed structure, by placing objects under the frame and thus stopping the displacement mechanism, we prevent the structure from entering this critical process.

In phase II, by applying voltage to the inner comb actuators, the upper capacitor plate continues moving downward by the inner springs.

In this case, when the inner comb drives are reached the critical point of the inner comb drive pull-in, at the same time the top capacitance plate will also travel the desired air gap ($g/2$) and touches the dielectric layer on the bottom capacitive plate. It is the maximum displacement rate of the top capacitive plate in phase II.

3. DESIGN

The aim of this research is to introduce two separate sets of electrostatic comb drives as vertical actuators to create variable capacitor with maximum tuning range. Figure 4

shows the total comb drive shape. As shown in this figure, when the voltage is applied, the movable comb will be displaced in the Z direction due to the fringing fields created in the comb. The capacitance between electrically conductive combs is expressed as:

$$C_{comb-drive} = N\epsilon_0 l(z + b_0) \left(\frac{1}{g-y} + \frac{1}{g+y} \right) \quad (1)$$

For equal distance between the plates the capacitance is expressed as:

$$C_{comb-drive} = N\epsilon_0 l(z + b_0) \left(\frac{2}{g} \right) \quad (2)$$

In Equation (2), ‘N’ indicates the number of combs, ‘l’ refers to the comb-length, ‘b₀’ is the initial overlap, ‘g’ is the adjacent gap size, ‘z’ is the vertical displacement amplitude along the z axis and ‘y’ represents the transversal displacement along the y axis. The energy stored in the capacitor is:

$$u_c = \frac{1}{2} C_{comb-drive}(z) V^2 \quad (3)$$

On the other hand, the electrostatic force applied to the comb drive is found by considering the power delivered to a time dependent capacitance and is given in the literature [37-39]:

$$f_z = \frac{d(w=u_c)}{dz} \quad (4)$$

By substitution:

$$F_{z1} = F_f = \frac{d\left(\frac{1}{2}C_{comb-drive}(z)V^2\right)}{dz} = \frac{1}{2}V^2 \frac{dC_{comb-drive}(z)}{dz} = \frac{1}{2}V^2 \frac{d\left[N\epsilon_0 l(z+b_0)\left(\frac{2}{g}\right)\right]}{dz} = \frac{1}{2}V^2 \left(\frac{2}{g}N\epsilon_0 l\right) = \frac{N\epsilon_0 l}{g}V^2 \quad (5)$$

The movable electrode on ground potential will be displaced in the z direction due to the fringe fields created in the comb. There is another capacitor which consists of the capacitor plate formed by the front end of the movable fingers and of the parallel part of the fixed electrode in front of it. This capacitance is expressed as:

$$C_{parallel-plate}(z) = 2N\epsilon_0 \frac{A}{(d-z)} \quad (6)$$

where ‘A’, ‘N’ and ‘d’ are the electrostatic area, number of fingers, and initial distance of the front ends of the

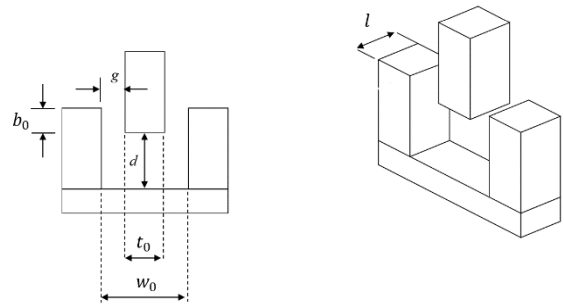


Figure 4. Schematic of comb drive structure

fingers if no actuation occurs and 'z' refers to the displacement in the z direction, respectively. The capacitor named by parallel plate capacitor does not have same electrodes. If we consider the electrostatic area of the front end of the movable fingers by $A_1 = l \times t_0$, and the parallel part area of the fixed electrode in front of movable electrode by $A_2 = l \times w_0$, then the capacitance is expressed as:

$$C_{parallel-plate}(z) = 4N\epsilon_0 \frac{A_1 A_2}{(d-z)(A_1+A_2)} \quad (7)$$

The corresponding parallel plate electrostatic force is given by:

$$F_{z2} = F_p = \frac{1}{2} \frac{dC_{parallel-plate}(z)}{dz} V^2 = \frac{1}{2} \frac{d}{dz} \left[2N\epsilon_0 l \frac{A}{(d-z)} \right] V^2 = \frac{1}{2} 2N\epsilon_0 l A \frac{d}{dz} \left[\frac{1}{(d-z)} \right] V^2 = \frac{N\epsilon_0 l A}{(d-z)^2} V^2 \quad (8)$$

For an actuator in equilibrium, two types of electrostatic forces can be considered. The total electrostatic force in the comb drive is expressed as:

$$F_e = F_z = F_{z1} + F_{z2} = F_f + F_p = \frac{N\epsilon_0 l}{g} V^2 + \frac{N\epsilon_0 l A}{(d-z)^2} V^2 \quad (9)$$

If the movable electrode is displaced, following the Hooke's law, the reaction force F_s , is generated:

$$F_s = k_z(d-z) \quad (10)$$

In this equation 'k_z' refers to equivalent spring constant in the 'z' direction. The springs used for both phases of proposed structure are of fixed-guided end type (Figure 5). Corresponding equation of this spring constant that is due to four fixed-guided end beams is given by Rebeiz [40]:

$$k_z = 4 \frac{Ewt^3}{l^3} \quad (11)$$

where, 'w', 't' and 'l' are width, thickness and length of the beams, respectively. In this equation 'k_z' refers to equivalent spring constant in the 'z' direction. Now, for the set of outer springs, we're going to have k_{z1} .

$$k_{z1} = 4 \frac{Ew_1 t_1^3}{l_1^3} \quad (12)$$

where, 'w₁', 't₁' and 'l₁' are width, thickness and length of the beams, respectively. In this equation 'k_{z1}' refers to equivalent spring constant in the 'z' direction; the spring constant is due to four outer fixed-guided end beams. These beams connect frame to anchors. And for the set of inner springs, k_{z2} .

$$k_{z2} = 4 \frac{Ew_2 t_2^3}{l_2^3} \quad (13)$$

where, 'w₂', 't₂' and 'l₂' are width, thickness and length of the beams, respectively. In this equation 'k_{z2}' refers to equivalent spring constant in the 'z' direction; the spring constant is due to four inner fixed-guided end beams. These beams connect top capacitance plate to frame. We

will now apply the final Equations (9) and (10) in the presented plan.

As mentioned in the description of the structure in the previous section, the proposed variable capacitor is designed to have two separate phases of motion and we also need to remember that the movement in each phase will be made by the specific comb drive actuators of that phase.

So, we can name the total electrostatic force in the outer combs (phase I) drive with F_{e1} :

$$F_{e1} = F_{f1} + F_{p1} = \frac{N\epsilon_0 l_1}{g} V_1^2 + \frac{N\epsilon_0 l_1 A_1}{(d-z)^2} V_1^2 \quad (14)$$

and subsequent, the reaction force with F_{s1} :

$$F_{s1} = k_{z1}(d-z) \quad (15)$$

Also these forces are F_{e2} :

$$F_{e2} = F_{f2} + F_{p2} = \frac{N\epsilon_0 l_2}{g} V_2^2 + \frac{N\epsilon_0 l_2 A_2}{(d-z)^2} V_2^2 \quad (16)$$

and F_{s2} :

$$F_{s2} = k_{z2}(d-z) \quad (17)$$

for the inner combs (phase II), respectively.

In equilibrium and by equating the applied electrostatic force (9) with the mechanical restoring force (10) the actuation voltage is achieved.

$$V = \sqrt{\frac{K_z(d-z)}{\frac{N\epsilon_0 h}{g} + 2N\epsilon_0 \frac{A_1 A_2}{(d-z)^2(A_1+A_2)}}} \quad (18)$$

Large tuning ratio together with low actuation voltage are the main goals of the proposed structure. The main parameter in determining the initial capacitance is its air-gap. Large tuning ratio requires large air-gap. For this reason 6μm air-gap is considered. On the other hand, low actuation voltage requires low spring constant together with small air-gap between the comb plates, long comb length and large area by considering Equation (18). Geometrical parameters in Table 1 satisfy our mentioned goals. Based on the parameters in Table 1 the outer and inner spring constant and by considering the equations 11, 12 and 13 are 0.11 and 0.72 N/m, respectively. The corresponding voltages due to these spring constants are 4 and 11V, respectively. To verify, the calculated results are again calculated using MATLAB software, and then simulated using Intellisuite software in the next section.

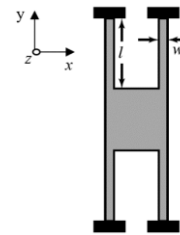


Figure 5. Schematic of fixed-guided end beam

4. CALCULATION AND SIMULATION RESULTS

As discussed in the previous section, the moving of the top capacitor plate to the bottom plate is done in two phases, phases I and II. For both phases, the calculated results for the proposed structure are again calculated using MATLAB software. Then, to validate the structure is simulated using Intellisuite software.

Materials and geometrical parameters of the structure is indicated in Table 1.

TABLE 1. Materials and geometrical parameters

Parameters	Value
Young’s modulus (Al)	74 GPa
Yield strength (Al)	310 MPa
Variable capacitor area	280um×280um
Movable capacitor plate thickness	2 um
Initial air gap of variable capacitor	6 um
Length of stopper	392 um
Width of stopper	40 um
Thickness of stopper	10 um
External dimension of frame	436um×436um
Width of frame	40um
Thickness of frame	6um
Parameters of Phase I	
Value	
Length of fixed-guided end beams	480 um
Width of fixed-guided end beams	40 um
Thickness of fixed-guided end beams	1 um
Length of combs	480 um
Width of combs	3 um
Thickness of combs	7 um
Number of Movable Combs	8
Initial distance of the front ends of the fingers	6 um
Lateral air gap between fingers	1 um
Parameters of Phase II	
Value	
Length of fixed-guided end beams	340 um
Width of fixed-guided end beams	43 um
Thickness of fixed-guided end beams	1 um
Length of combs	80 um
Width of combs	3 um
Thickness of combs	7 um
Nmber of Movable Combs	20
Initial distance of the front ends of the fingers (at the end of Phase I)	6 um
Lateral air gap between fingers	1 um

Now we consider phase I. Figure 6 shows calculation results of movable capacitor plate displacement versus applied voltage. It should be noted again, that the voltage is applied to the combs. These combs are connected to the capacitor movable plate. As it is seen from the figure, the total capacitor movable plate displacement and corresponding voltage before snapping is 3.6um and 3.6V, respectively. To verify, the proposed structure is simulated using Intellisuite software. Figure 7 shows simulation result of the structure.

As it is seen, the calculation results is approximately the same as the simulation results. Figure 8 shows the maximum displacement (3um) of the movable plate due to the required applied voltage. At this point the frame is stopped as a result of the collision with the stopper. Therefore, phase I displacement mechanism ends. Figures 9 and 10 show calculated and simulated results of capacitance versus different applied voltages in phase I. As it is seen, the calculation result is approximately the same as the simulation result.

Figure 11 shows induced stress in the structure due to applied voltage and consequently the displacement of movable section.

If the voltage is removed, the mentioned stress is also removed. There is another stress due to fabrication process. This stress is named by "residual stress". Figures 12 and 13 show the effect of 20 MPa and 40 MPa residual stresses on the applied voltage. As it is seen the pull-in voltage is increased.

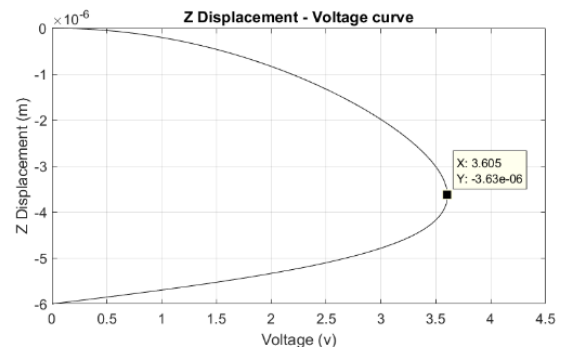


Figure 6. Calculated result of movable capacitor plate versus applied voltages (phase I)

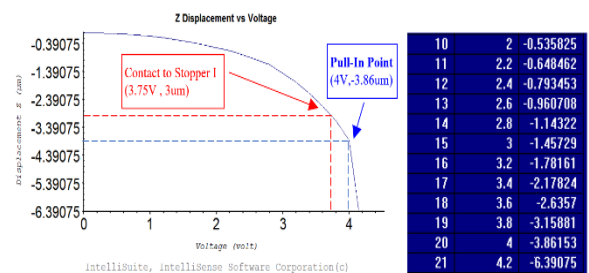


Figure 7. Simulated result of movable capacitor plate versus applied voltages (phase I)

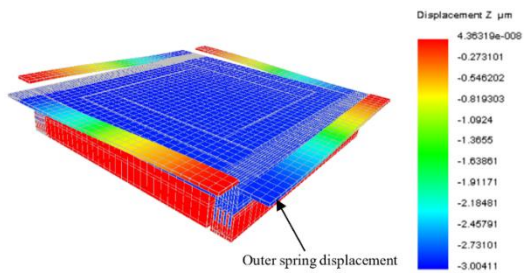


Figure 8. Maximum displacement of capacitor movable plate in phase I

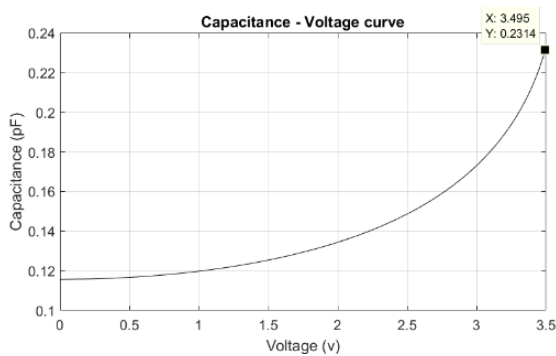


Figure 9. Calculated result of capacitance versus different applied voltages (phase I)

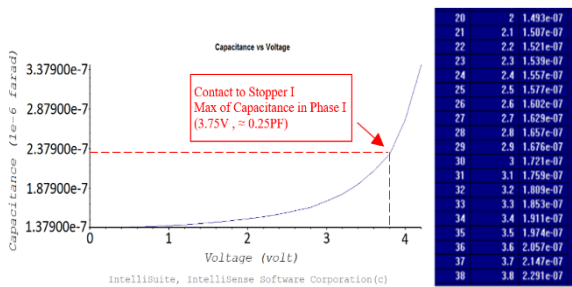


Figure 10. simulated result of capacitance versus different applied voltages (phase I)

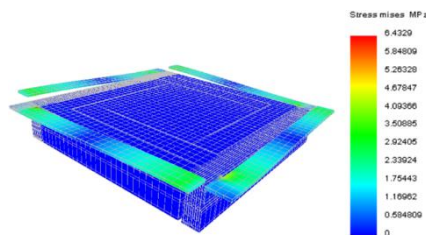


Figure 11. Stress mises_Residual Stress=0Mpa (phase I)

Figure 14 shows the effect of only stress on the air gap. As it is seen, simulation result show 0.02 μm capacitor plate displacement due to residual stress. The effect of mentioned displacement in the initial (minimum) capacitance is negligible.

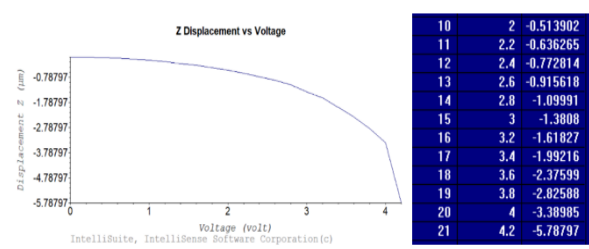


Figure 12. Simulated result of movable capacitor plate versus applied voltages_Residual Stress=20MPa (phase I)

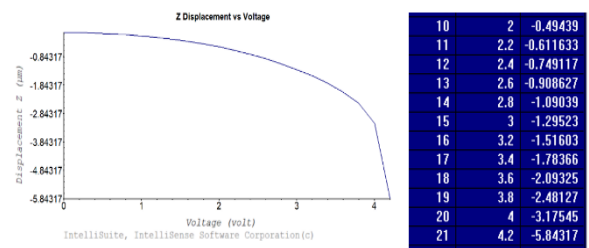


Figure 13. Simulated result of movable capacitor plate versus applied voltages_Residual Stress=40MPa (phase I)

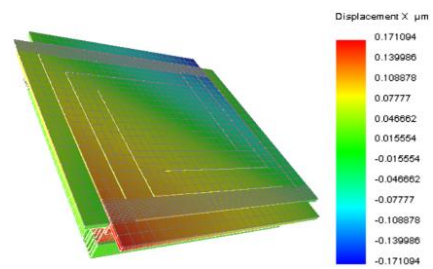


Figure 14.a Displacement along the x-axis due to Residual Stress=40Mpa in phase I

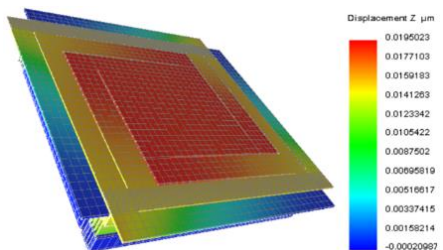


Figure 14.b Displacement along the z-axis due to Residual Stress=40Mpa in phase I

Now we consider phase II. Figure 15 shows calculation results of the movable capacitor plate displacement versus applied voltage. It should be noted again, that the voltage is applied to the combs. These combs are connected to the capacitor movable plate. As it is seen from the figure, the total capacitor movable plate displacement and corresponding voltage before snapping is 3.6 μm and 12.33V, respectively. To verify, the proposed structure is simulated using Intellisuite

software. Figure 16 shows simulation result of the structure. As it is seen, calculation result is approximately the same as the simulation result.

Figure 17 shows the maximum displacement ($3\mu\text{m}$) of the movable plate due to 63rd required applied voltage in phase II. At this point, the movable plate is stopped because of the collision with the dielectric layer on the capacitor fixed plate. Therefore, Phase II displacement mechanism ends. Figures 18 and 19 show calculated and simulated results of capacitance versus different applied voltages in phase II. As it is seen, the calculation result is approximately the same as the simulation result.

Figure 20 shows induced stress in the structure due to applied voltage and consequently the displacement of movable section. If the voltage is removed, the mentioned stress is also removed. Figures 21 and 22 show the effect of 20 and 40 MPa residual stresses on the

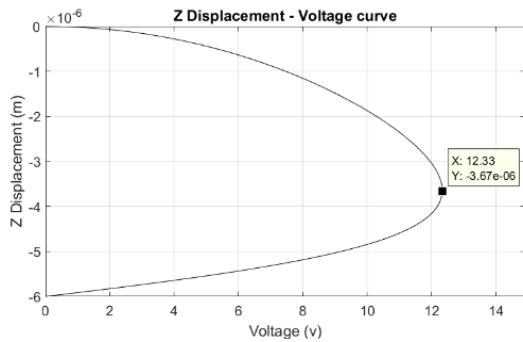


Figure 15. Calculation result of movable capacitor plate versus applied voltages (phase II)

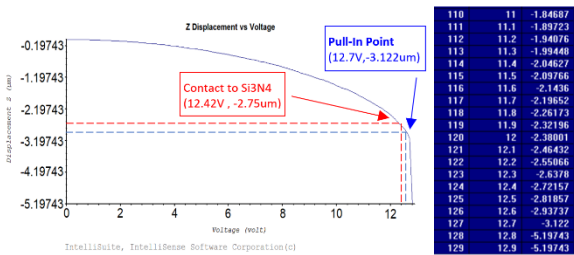


Figure 16. Simulation result of movable capacitor plate versus applied voltages (phase II)

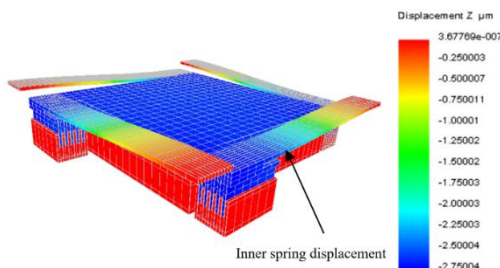


Figure 17. Maximum displacement of the capacitor movable plate in phase II

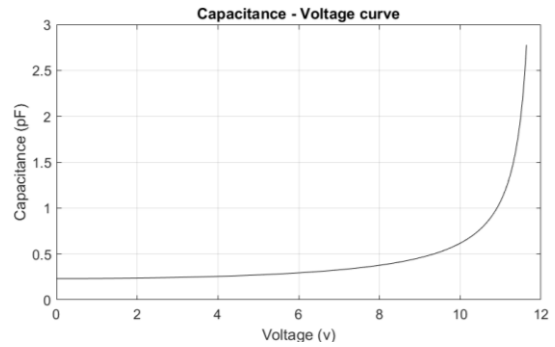


Figure 18. Calculated result of capacitance versus different applied voltages (phase II)

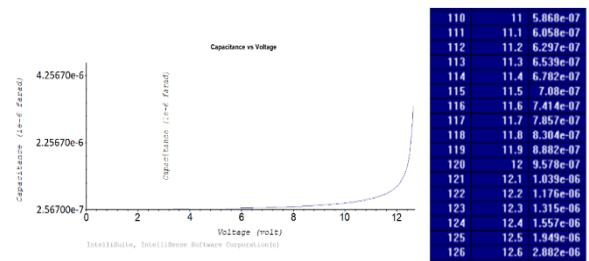


Figure 19. Simulated result of capacitance versus different applied voltages (phase II)

applied voltage. As it is seen the pull-in voltage is increased.

Figure 23 shows the effect of residual stress on the structure in phase II. Simulation result show $0.124\ \mu\text{m}$ and $0.028\ \mu\text{m}$ capacitor plate displacement due to residual stress in the y and z direction respectively. As it can be seen, the effect of mentioned displacement in the initial capacitance (Z direction) is small.

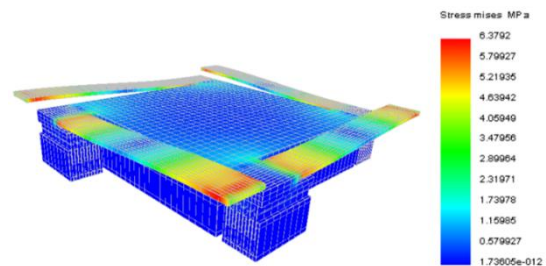


Figure 20. Stress mises (phase II)

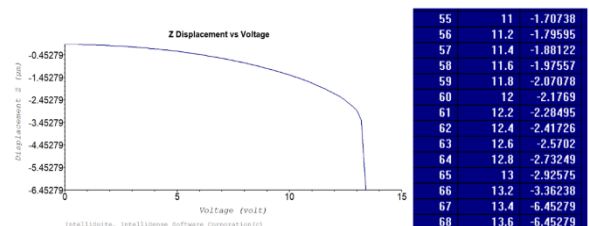


Figure 21. Simulated result of movable capacitor plate versus applied voltages_ Residual Stress=20MPa (phase II)

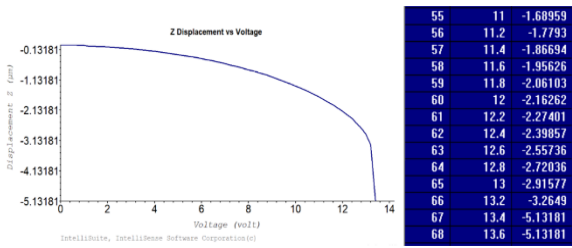


Figure 22. Simulated result of movable capacitor plate versus applied voltages_Residual Stress=40MPa (phase II)

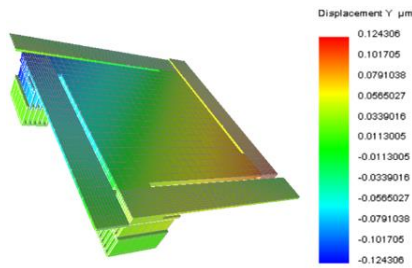


Figure 23.a Displacement due to Residual Stress=40Mpa in phase II - y direction

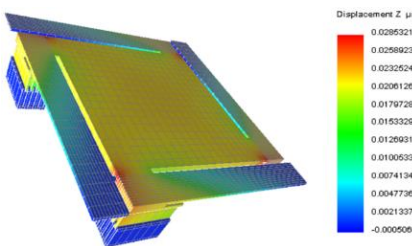


Figure 23.b Displacement due to Residual Stress=40Mpa in phase II - z direction

5. TUNING RANGE AND COMPARISON

The tuning range for a capacitor is the ratio of the difference between the maximum and minimum capacitance to its minimum capacitance that is expressed in percentage and is as follows:

$$Tuning\ range = \frac{C_{max} - C_{min}}{C_{min}} \times 100 \quad (19)$$

The calculated results of minimum and maximum capacitance from Figures 9 and 20 are 0.12Pf and 2.9Pf, respectively. The tuning range related to these capacitances is 2316%. To verify, the simulation is done. The simulated results of minimum and maximum capacitance from Figures 10 and 21 are 0.137 and 3.4 Pf, respectively. The tuning range related to these capacitances is 2380%.

Table 2 summarizes the comparison between our proposed structure and the one plate moveable counterpart. This comparison is based on some important

specifications such as tuning range, initial capacitance, actuation voltage and the effective capacitor size.

6. PROPOSED FABRICATION PROCESS

Fabrication steps of the proposed structure are shown in Figure 24. At first a high resistance substrate (SiO₂) is selected to prevent electrical connection between the different parts of the structure. Then, 0.1 μm layer of Al is deposited by sputtering and patterned to define lower plate of capacitor, anchors of external fixed-guided end beams, stoppers and outer and inner fixed combs as shown in Figure 24a. Next, a 0.1 μm silicon–nitride as a dielectric layer is deposited and patterned as shown in Figure 24b. In the third step a 6 μm polyimide 2526 as a sacrificial layer is deposited and patterned, to define inner and outer fixed combs by aluminum electroplating (Figure 24c). Then 1 μm aluminum is deposited by sputtering and patterned to create outer movable combs and overlap region of outer fixed and movable combs. Also the growth of the inner fixed combs is done (Figure 24d). To create the same level the other area in step four is filled with polyimide 2526. In the next step, 2 μm polyimide 2562 as a sacrificial layer and as a mold for aluminum electroplating is deposited, patterned and electroplated to define lower plate of capacitor, stoppers, outer movable combs and anchors of fixed-guided end beams (Figure 24e). Then 1 μm aluminum is deposited by sputtering and patterned to create inner movable combs, lower plate of capacitor, outer movable combs and anchors (Figure 24f). Then a 2 μm polyimide 2526 as a sacrificial layer and as a mold for aluminum

TABLE 2. MEMS variable capacitor performance comparison with the previously published variable capacitor

References No.	Tuning Rang	Initial Capacitance	Cmax	Actuation Voltage
[21]	41 %	0.3 PF	---	5.5 V
[6]	309 %	0.077 PF	0.238 PF	---
[22]	320 %	3 PF	---	13 V
[36]	242 %	1.955 PF	6.693 PF	9 V
[30]	207 %	24.5 fF	75.6 fF	40 V
[16]	286 %	0.498 PF	4.103 PF	28 V
[23]	240 %	15 PF	---	3.5 V
[20]	300 %	1.33PF	---	1.36 V
This Work (calculation)	2316 %	0.12 PF	2.9 PF	12.33V (without residual stress)
This Work (simulation)	2380%	0.137 PF	3.4 PF	12.42V (without residual stress)

electroplating is deposited patterned and electroplated to define lower plate of variable capacitor, inner and outer movable combs, and anchors (Figure 24g). Next, a $0.25 \mu\text{m}$ silicon-nitride as a dielectric layer is deposited and patterned as shown in Figure 24h. Then, a $1 \mu\text{m}$ polyimide 2526 as a sacrificial layer and as a mold for aluminum electroplating is deposited patterned and electroplated to define inner and outer movable combs and anchors (Figure 24i). In the tenth step a $3 \mu\text{m}$ polyimide 2526 as a sacrificial layer is deposited and patterned, to define frame by aluminum electroplating. The growth of the combs is done for the last time, while the growth of anchors continues (Figure 24j). Then $1 \mu\text{m}$ aluminum is deposited by sputtering and patterned to create frame, up electrode of movable combs and anchors (Figure 24k). Then $1 \mu\text{m}$ aluminum is deposited by sputtering and patterned to create frame, anchors and interconnection between up electrode of movable combs (Figure 24l). Then $1 \mu\text{m}$ aluminum is deposited by sputtering and patterned to create upper plate of variable capacitor, frame, outer fixed-guided end beams, inner fixed-guided end beams and anchors (Figure 24m). Finally, isotropic plasma ashing is used to remove sacrificial layer (Figure 24n).

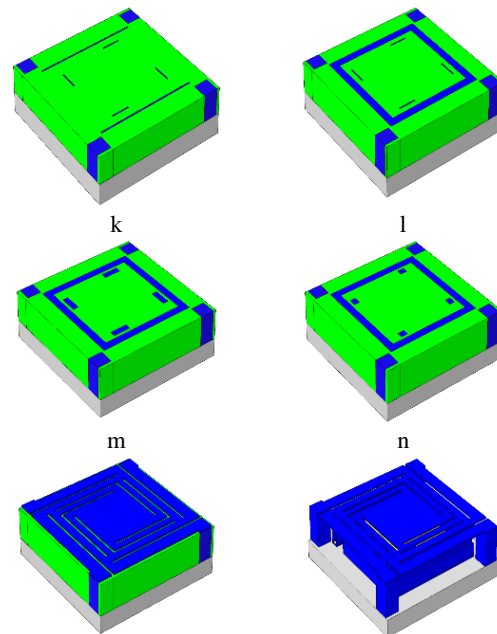
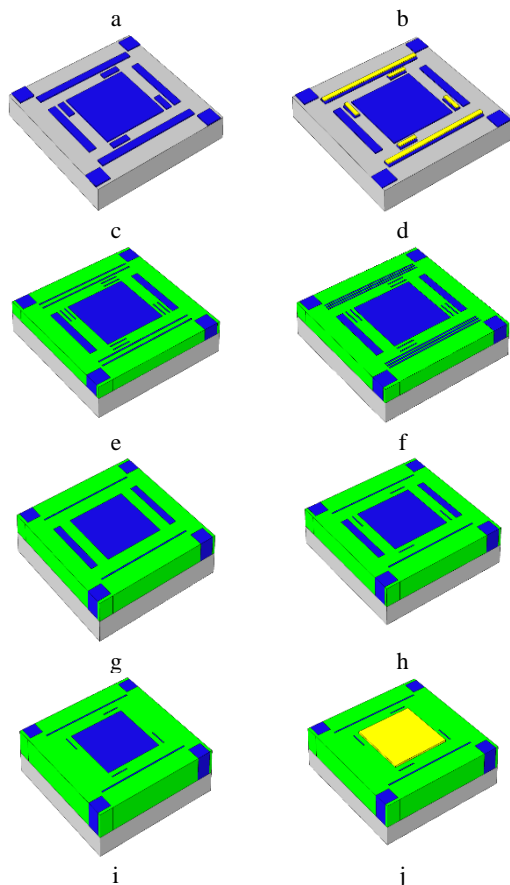


Figure 24. Schematic of proposed fabrication process



7. CONCLUSION

A new structure of MEMS variable capacitor was proposed to achieve maximum capacitance variation. It was accomplished by two independent displacement phases. In each phase, half of the desired final displacement was done and it was realized by special vertical comb drive actuators of that phase. In the second phase of displacement and for the first time, we introduced a new method in which the movable comb drive actuators are connected to the bottom of the guided end side of the inner guided end beams. Therefore, for the second mechanism of displacement, there is no need to increase the additional structure. The proposed structure was designed and then tested with MATLAB software. To verify, the structure was simulated using Intellisuite software. The achieved minimum tuning range and maximum applied voltage in the proposed structure is 2300% and 12.42V respectively.

8. REFERENCES

1. Dec, A. and Suyama, K., "Microwave mems-based voltage-controlled oscillators", *IEEE Transactions on Microwave Theory and Techniques*, Vol. 48, No. 11, (2000), 1943-1949. DOI: [10.1109/22.883875](https://doi.org/10.1109/22.883875)
2. Khodapanahandeh, M., Mirzajani, H. and Ghavifekr, H.B., "A novel electrostatically actuated high q rf mems tunable capacitor for uhf applications", in *Electrical Engineering (ICEE), Iranian Conference on*, IEEE. (2018), 11-16. DOI: [10.1109/ICEE.2018.8472482](https://doi.org/10.1109/ICEE.2018.8472482)

3. Rebeiz, G.M., Tan, G.-L. and Hayden, J.S., "Rf mems phase shifters: Design and applications", *IEEE Microwave Magazine*, Vol. 3, No. 2, (2002), 72-81. DOI: [10.1109/MMW.2002.1004054](https://doi.org/10.1109/MMW.2002.1004054)
4. Saberhosseini, S.S., Ganji, B.A., Koohsorkhi, J. and Ghorbani, A., "Design and simulation of a variable mems capacitor for tunable hmsiw resonator", *IET Circuits, Devices & Systems*, Vol. 14, No. 5, (2020), 707-712. doi: [10.1049/iet-cds.2019.0511](https://doi.org/10.1049/iet-cds.2019.0511)
5. Reinke, J.R., "Cmos-mems variable capacitors for reconfigurable rf circuits", Carnegie Mellon University, Ph.D. Thesis (2011),
6. Gong, Z., Liu, H., Guo, X. and Liu, Z., "Optimization of a mems variable capacitor with high linearity and large tuning ratio", *Microsystem Technologies*, Vol. 24, No. 7, (2018), 3169-3178. doi.org/10.1007/s00542-018-3844-z
7. Gupta, P., Singh, P. and Srivastava, P., "Design and analysis of rf mems varactor for extended tuning range", in 2013 International Conference on Control, Computing, Communication and Materials (ICCCCM), IEEE. (2013), 1-4. DOI: [10.1109/ICCCCM.2013.6648915](https://doi.org/10.1109/ICCCCM.2013.6648915)
8. Mobki, H., Rashvand, K., Afrang, S., Sadeghi, M.H. and Rezazadeh, G., "Design, simulation and bifurcation analysis of a novel micromachined tunable capacitor with extended tunability", *Transactions of the Canadian Society for Mechanical Engineering*, Vol. 38, No. 1, (2014), 15-29. doi.org/10.1139/tcsme-2014-0002
9. Mohabbatian, N., Abbaspour-Sani, E. and Ghasemzadeh, M., "An electrostatic tunable rf mems capacitor with improved quality factor", in 2014 22nd Iranian Conference on Electrical Engineering (ICEE), IEEE. (2014), 422-427. DOI: [10.1109/IranianCEE.2014.6999577](https://doi.org/10.1109/IranianCEE.2014.6999577)
10. Nguyen, H., Hah, D., Patterson, P.R., Piyawattanametha, W., Wu, M.C. and Chao, R., "A novel mems tunable capacitor based on angular vertical comb drive actuators", in Solid-State Sensor, Actuator and Microsystems Workshop, Citeseer. (2002), 277-280.
11. Rijks, T.G., Van Beek, J., Steeneken, P., Ulenaers, M., De Coster, J. and Puers, R., "Rf mems tunable capacitors with large tuning ratio", in 17th IEEE International Conference on Micro Electro Mechanical Systems. Maastricht MEMS 2004 Technical Digest, IEEE. (2004), 777-780. DOI: [10.1109/MEMS.2004.1290700](https://doi.org/10.1109/MEMS.2004.1290700)
12. Teymoori, M.M., Ahangarkolaei, J.M. and Sangrody, R.A., "Investigation and comparison of two movable plates electrostatic mems tunable capacitors", *International Journal of Electronics Communication and Computer Engineering*, Vol. 6, No. 3, (2015), 404-408.
13. Feng, Z., Zhang, W., Su, B., Harsh, K.F., Gupta, K., Bright, V. and Lee, Y., "Design and modeling of rf mems tunable capacitors using electro-thermal actuators", in 1999 IEEE MTT-S International Microwave Symposium Digest (Cat. No. 99CH36282), IEEE. Vol. 4, (1999), 1507-1510. DOI: [10.1109/MWSYM.1999.7802401](https://doi.org/10.1109/MWSYM.1999.7802401)
14. Lee, C.-Y. and Kim, E.S., "Piezoelectrically actuated tunable capacitor", *Journal of Microelectromechanical Systems*, Vol. 15, No. 4, (2006), 745-755. DOI: [10.1109/JMEMS.2006.878886](https://doi.org/10.1109/JMEMS.2006.878886)
15. Mehran, M., Rotani, E.Z., Shirazi, A.D.M. and Hakimi, A., "An electro-thermal mems variable capacitor", in 2020 28th Iranian Conference on Electrical Engineering (ICEE), IEEE. Vol., No. Issue, (2020), 1-5. DOI: [10.1109/ICEE50131.2020.9260576](https://doi.org/10.1109/ICEE50131.2020.9260576)
16. Shahi, M., "Development of tunable mems capacitor with dual-mode deformation to improve tunability and linearity", Southern Illinois University at Edwardsville, (2021), M.Sc. Thesis
17. Nguyen, H.D., Hah, D., Patterson, P.R., Chao, R., Piyawattanametha, W., Lau, E.K. and Wu, M.C., "Angular vertical comb-driven tunable capacitor with high-tuning capabilities", *Journal of Microelectromechanical Systems*, Vol. 13, No. 3, (2004), 406-413. DOI: [10.1109/JMEMS.2004.828741](https://doi.org/10.1109/JMEMS.2004.828741)
18. Steeneken, P., Rijks, T.G., Van Beek, J., Ulenaers, M., De Coster, J. and Puers, R., "Dynamics and squeeze film gas damping of a capacitive rf mems switch", *Journal of Micromechanics and Microengineering*, Vol. 15, No. 1, (2004), 176.
19. Li, Z. and Tien, N.C., "A high tuning-ratio silicon-micromachined variable capacitor with low driving voltage", in Proc. Solid-State Sensor and Actuator Workshop. (2002), 2-6.
20. Ashoori, M. and Nabovati, H., "Wide tuning range and high quality factor mems variable capacitor with two movable plates in 0.18 μm cmos technology", *Majlesi Journal of Mechatronic Systems*, Vol. 3, No. 4, (2014), 25-31.
21. Lee, H.S., Yoon, Y.J., Choi, D.-H. and Yoon, J.-B., "High-q, tunable-gap mems variable capacitor actuated with an electrically floating plate", in 2008 IEEE 21st International Conference on Micro Electro Mechanical Systems, IEEE. (2008), 180-183. DOI: [10.1109/MEMSYS.2008.4443622](https://doi.org/10.1109/MEMSYS.2008.4443622)
22. Li, X., Xia, Y., Liu, J., Yin, L., Liu, Y., Fang, D. and Zhang, H., "Tunable rf mems capacitor for wireless communication", in 2009 International Conference on Optical Instruments and Technology: MEMS/NEMS Technology and Applications, International Society for Optics and Photonics. Vol. 7510, (2009), 751002. <https://doi.org/10.1117/12.845903>
23. Rais-Zadeh, M., Samaroo, A., Monajemi, P. and Ayazi, F., "Low-voltage large-value tunable capacitors using selfaligned harpss", in 2008 IEEE 21st International Conference on Micro Electro Mechanical Systems, IEEE. (2008), 319-322. DOI: [10.1109/MEMSYS.2008.4443657](https://doi.org/10.1109/MEMSYS.2008.4443657)
24. Al-Ghamdi, M., Khater, M., Abdel-Rahman, E. and Nepomuceno, E., "Quasi-static pull-in: An instability in electrostatic actuators", *Scientific Reports*, Vol. 10, No. 1, (2020), 1-8. doi.org/10.1038/s41598-020-61534-w
25. Azizi, A., Fard, N.M., Mobki, H. and Arbi, A., "Bifurcation behaviour and stability analysis of a nano-beam subjected to electrostatic pressure", *Applied and Computational Mathematics*, Vol. 7, No. 1-2, (2018), 1-11.
26. Razeghi A., B. Azizollah Ganji; A. Abdipour; R. A. Jafari-Talookolaei., "A Novel Metamaterial Microelectromechanical Systems Phase Shifter with High Phase Shift and High Bandwidth", *International Journal of Engineering, Transactions B: Applications*, Vol. 32, No. 8, (2019) 1163-1168 doi: [10.5829/ije.2019.32.08b.12](https://doi.org/10.5829/ije.2019.32.08b.12)
27. Prathier, B., "Electrostatically driven mems resonator: Pull-in behavior and non-linear phenomena", *Nonlinear Systems: Theoretical Aspects and Recent Applications*, (2020), 241.
28. Rezazadeh, G., Rashvand, K. and Madineh, H., "Effect of length-scale parameter on pull-in voltage and natural frequency of a micro-plate", *International Journal of Engineering, Transactions C: Aspects*, Vol. 27, No. 3, (2014), 375-384. doi: [10.5829/idosi.ije.2014.27.03c.04](https://doi.org/10.5829/idosi.ije.2014.27.03c.04)
29. Zhang, W.-M., Yan, H., Peng, Z.-K. and Meng, G., "Electrostatic pull-in instability in mems/nems: A review", *Sensors and Actuators A: Physical*, Vol. 214, (2014), 187-218. doi.org/10.1016/j.sna.2014.04.025
30. Afrang, S., Mobki, H., Sadeghi, M.H. and Rezazadeh, G., "A new mems based variable capacitor with wide tunability, high linearity and low actuation voltage", *Microelectronics Journal*, Vol. 46, No. 2, (2015), 191-197. doi.org/10.1016/j.mejo.2014.11.006
31. Bakri-Kassem, M. and Mansour, R., "High tuning range parallel plate mems variable capacitors with arrays of supporting beams", in 19th IEEE international conference on micro electro mechanical systems, IEEE. (2006), 666-669. DOI: [10.1109/MEMSYS.2006.1627887](https://doi.org/10.1109/MEMSYS.2006.1627887)
32. McFeetors, G. and Okoniewski, M., "Performance and operation of stressed dual-gap rf mems varactors", in 2006 European Microwave Conference, IEEE. (2006), 1064-1067. DOI: [10.1109/EUMC.2006.281117](https://doi.org/10.1109/EUMC.2006.281117)

33. Mobki, H., Sadeghi, M.H., Afrang, S. and Rezazadeh, G., "On the tunability of a mems based variable capacitor with a novel structure", *Microsystem Technologies*, Vol. 17, No. 9, (2011), 1447-1452. doi.org/10.1007/s00542-011-1327-6
34. Rezazadeh, G. and Mobki, H., "Application of thau observer for fault detection of micro parallel plate capacitor subjected to nonlinear electrostatic force", *International Journal of Engineering, Transactions B: Applications*, Vol. 28, No. 2, (2015), 270-276. doi: 10.5829/idosi.ije.2015.28.02b.13
35. Borwick, R.L., Stupar, P.A., DeNatale, J.F., Anderson, R. and Erlandson, R., "Variable mems capacitors implemented into rf filter systems", *IEEE Transactions on Microwave Theory and Techniques*, Vol. 51, No. 1, (2003), 315-319. DOI: 10.1109/TMTT.2002.806519
36. Afrang, S. and Nematkhah, N., "A new mems based variable capacitor using electrostatic vertical comb drive actuator and auxiliary cantilever beams", *Microsystem Technologies*, Vol. 25, No. 9, (2019), 3317-3327. DOI: 10.1109/TMTT.2002.806519
37. Chen, C. and Lee, C., "Design and modeling for comb drive actuator with enlarged static displacement", *Sensors and Actuators A: Physical*, Vol. 115, No. 2-3, (2004), 530-539. doi.org/10.1016/j.sna.2004.04.052
38. Jaecklin, V., Linder, C., De Rooij, N. and Moret, J., "Micromechanical comb actuators with low driving voltage", *Journal of Micromechanics and Microengineering*, Vol. 2, No. 4, (1992), 250.
39. Legtenberg, R., Groeneveld, A. and Elwenspoek, M., "Comb-drive actuators for large displacements", *Journal of Micromechanics and Microengineering*, Vol. 6, No. 3, (1996), 320.
40. Rebeiz, G.M., "Rf mems: Theory, design, and technology, John Wiley & Sons, (2004).

Persian Abstract

چکیده

این مقاله یک خازن متغییر بر پایه فن آوری MEMS برای رسیدن به یک ناحیه پایدار بزرگ و قابلیت تنظیم وسیع را ارائه می کند. ایده کار بر اساس افزایش ناحیه پایدار در فاصله هوایی بین صفحات خازنی است که با ترکیب عملکرد دو مجموعه محرک شانه ای عمودی انجام می گیرد تا به تغییرات فاصله هوایی واحد غلبه شود. طراحی ساختار به صورتی است که عملکرد این دو مجموعه محرک، کاملاً مستقل از یکدیگر و بدون تداخل و یا تخریب روی هم انجام شود. برتری طرح در این است که اضافه کردن مکانیزم دوم تحریک، ضخامت کلی ساختار را تغییر نمی دهد در مقایسه با حالتی که ساختار فقط از یک مکانیزم تحریک استفاده می کند. بنابراین قابلیت تنظیم شدیداً افزایش می یابد. ماده پایه مورد استفاده برای طراحی، آلومینیوم است. محرک های شانه های به صورت وسیع به عنوان موتورهای MEMS بکار برده می شوند، به علت محدوده وسیع حرکت خطی، مصرف توان پایین و سادگی فرآیند ساخت آنها. یک بررسی کامل از محرک های الکترواستاتیک انجام شده است. ساختار با استفاده از نرم افزار MATLAB محاسبه شده است. برای تایید، نتایج محاسبه شده با نتایج شبیه سازی حاصل شده از نرم افزار Intellisuit مقایسه شده است. فرکانس طبیعی ساختار 1.173KHZ می باشد. مطابق با نتایج محاسبات و شبیه سازی، محدوده تنظیم بدست آمده 2300% است.
